A Novel Compact Torsional Spring for Series Elastic Actuators for Assistive Wearable Robots

Giorgio Carpino, Dino Accoto*, Fabrizio Sergi, Nevio Luigi Tagliamonte and Eugenio Guglielmelli
Laboratory of Biomedical Robotics and Biomicrosystems
Center for Integrated Research
University Campus Bio-Medico di Roma
via Álvaro del Portillo, 21
Rome, 00128
Italy
Email: g.carpino@unicampus.it

The introduction of intrinsic compliance in the actuation system of assistive robots improves safety and dynamical adaptability. Furthermore, in the case of wearable robots for gait assistance, the exploitation of conservative compliant elements as energy buffers can mimic the intrinsic dynamical properties of legs during locomotion. However, commercially available compliant components do not generally allow to meet the desired requirements in terms of admissible peak load, as typically required by gait assistance, while guaranteeing low stiffness and a compact and lightweight design. This paper presents a novel compact monolithic torsional spring to be used as the basic component of a modular compliant system for Series Elastic Actuators. The spring, whose design was re ned through an iterative FEA-based optimization process, has an external diameter of 85 mm, a thickness of 3 mm and a weight of 61.5 g. The spring, characterized using a custom dynamometric test bed, shows a linear torque vs. angle characteristic. The compliant element has a stiffness of 98 N·m/rad and it is capable of withstanding a maximum torque of 7.68 N·m. A good agreement between simulated and experimental data was observed, with a maximum resultant error of 6%. By arranging a number of identical springs in series or in parallel, it is possible to render different torque vs. angle characteristics, in order to match the speci c applications requirements.

Keywords*: Series Elastic Actuator, torsional spring, pHRI, wearable robot*

1 Introduction

Robots, especially those intended for industrial environments, have been classically designed according to the principle "rigidity by design, safety by sensors and control". In assistive, rehabilitation and service robotics, where physical Human-Robot Interaction (pHRI) is central, the paradigm "safety by design, performance by control" was established as the most appropriate to assure that satisfactory safety levels are reached [1]. The assistance to human movements should be imparted by regulating interaction forces, thus avoiding to rigidly move subjects limbs according to prescribed kinematic patterns. The need to stably and robustly regulate human-robot dynamic interaction, also considering the variable assistance level required by different subjects, entails the use of actuators operating in an ideal force (or torque) mode control. This implies theoretical zero output impedance (i.e. perfect back-drivability) and high force (or torque) control fidelity. One possible approach to improve the level of adaptability and safety resorts to the inclusion of intrinsic compliance in the actuation system.

Several actuation solutions have been proposed to meet such requirements [2]. The Series Elastic Actuator (SEA) architecture is a simple and effective solution, which basically consists of a gearmotor in series to a spring connected to the load [3, 4]. This architecture allows to decouple the output from motor inertia and other non-linearities, with benefits in terms of force (or torque) control fidelity. Additionally, the force exerted on the load can be simply evaluated by measuring the deflection of the elastic element. The intrinsic compliance guarantees low impedance across the whole frequency spectrum: for external perturbations at frequencies above the actuator controllable bandwidth, the impedance of the system reduces to the stiffness of the spring, thus avoiding unsafe behaviors due to sensors failure and/or control bandwidth limitation. It can be demonstrated [4] that a higher compliance in the torque control loop allows increasing the control gains within fixed stability margins. This results in a reduction of the effects of internal stiction and other transmission non-linearities (friction and backlash) and in an improvement of the torque tracking performance. In [5] it has also been proved that the adequate selection of spring stiffness, according to a specific application, can lead to an

*Giorgio Carpino and Dino Accoto equally contributed to this work and should be considered co-first authors.

energetic optimization of the system. The major drawback introduced by the series elastic element is the reduction of the actuator bandwidth [6]: a higher compliance of the actuator reduces the bandwidth of the torque control. A direct consequence of this behavior is that, given a target torque control specification, a SEA might require extra power with respect to a traditional stiff motor. Moreover, when the system is stiffness-controlled (i.e. it mimics an elastic behavior) and conservative stability constraints have to be met, the maximum stiffness that can be rendered is limited to the physical stiffness of the elastic element [7].

SEAs were originally employed in bipedal walking and running robots [8] where unavoidable high frequency disturbances, due to impacts with the ground, must be rejected. SEAs are now widely adopted also in wearable robotics for gait assistance [9, 10]. In this application, where a typical actuation cycle consists of a sequence of concentric (positive power transfer from the actuator to the load) and eccentric (negative power transfer) phases, the property of compliant elements to serve as energy buffers can be exploited to reduce the overall actuator power demands. The system proposed in [3, 4] is a linear actuator but a number of rotary prototypes have been recently developed for different applications [9–16].

A typical torque control for SEAs is depicted in the simplified scheme in Fig. 1. The spring deflection $\Delta\theta$ provides an estimate of the torque exerted by the actuator τ_l. This measure is used as the feedback signal for the torque control, which becomes a simpler (especially in the case of a linear stiffness) position control, where the equilibrium position of the spring is continuously varied for torque regulation. The stiffness of the series elastic element must be carefully selected in order to trade off between performances, adaptability and safety, as it will be shown in the next sections. Dimensions and weight must be reduced as much as possible, especially for wearable robotics applications. Moreover, the elastic element should be directly connected to the load to avoid the effect of force-fidelity reduction caused by transmission non-linearities.

From a mechanical perspective, the main challenge in the design of compliant elements for SEAs is the achievement of low stiffness while guaranteeing an adequate robustness with respect to high torques (in the order of 10-50 N·m for typical applications in assistive robotics).

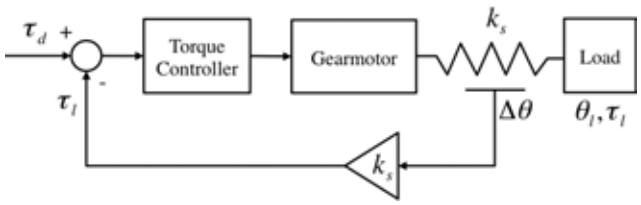

Fig. 1. General torque control scheme for a rotary SEA. τ_d represents the desired torque, k_s the spring stiffness, $\Delta\theta$ the spring deflection, τ_l the output torque and θ_l the output angle.

1.1 State of Art of Torsional Springs for SEAs

A considerable amount of research in SEA development has been focused on designing custom components suitable to match the specific requirements of a given application. It can be useful to group the compliant components of SEAs in two different classes, depending on the solutions adopted to implement the desired output torsional stiffness. The first class comprises compliant systems adopting linear compression springs arranged in such a way that a centering elastic torque is produced when the joint shaft is rotated [9, 11–13]. The second class includes compliant systems employing torsional springs embedded in the transmission train [10], or custom torsional springs directly connected to the load [14–16].

Let's take into account the first class. A system with a three-spoke output component, a circular input pulley and six linear springs was presented in [11] (Fig. 2–A). A similar approach, where six linear springs are used, is described in [12] (Fig. 2–B). In [13, 18] four springs have been used to render a torsional stiffness as needed to develop a velocity sourced SEA. In the SEA described in [9,17], the torsional elastic behavior is demanded to the agonistic-antagonistic configuration of two linear compression springs connected to the actuator disk by a cable (Fig. 2–C); the two compression springs are pre-tensioned with the maximally desired force, so that the connecting cable is always under tension during operation.

The springs included in the systems belonging to the second class can be either commercial or custom. In the first case the spring can be embedded in the power transmission line, as in [10] (Fig. 2–D). Here the spring is mounted between the worm gear and the output gears. However, some loss of force transfer fidelity occurs due to the non-linearities associated to output gears. This drawback can be circumvented by directly placing the spring between the gearmotor and the load. This solution usually implies the development of custom elastic components. In [14] a custom-made double spiral spring, in series with a frameless motor, is presented (Fig. 2–E), based on a previous design [15]. The double spiral design cancels out undesired radial forces acting on the spring center when the spring is deformed by a torque. Another design is described in [16] (Fig. 2–F), where a custom spiral shaped unidirectional torsional spring has been implemented in the biped robot Kurmet.

1.2 Objectives

The goal of the present work is to describe the development of a compact, monolithic, torsionally compliant element, that can be included in the actuator of a wearable robot for knee assistance. The target application requires a design focused on the simultaneous achievement of two objectives: *i)* the capability of providing the assistive torque necessary to support human locomotion with a low intrinsic stiffness and *ii)* the minimization of the resulting weight and dimensions (see Section 2).

The selection of the physical stiffness of the series elastic component has an impact on actuator performance and

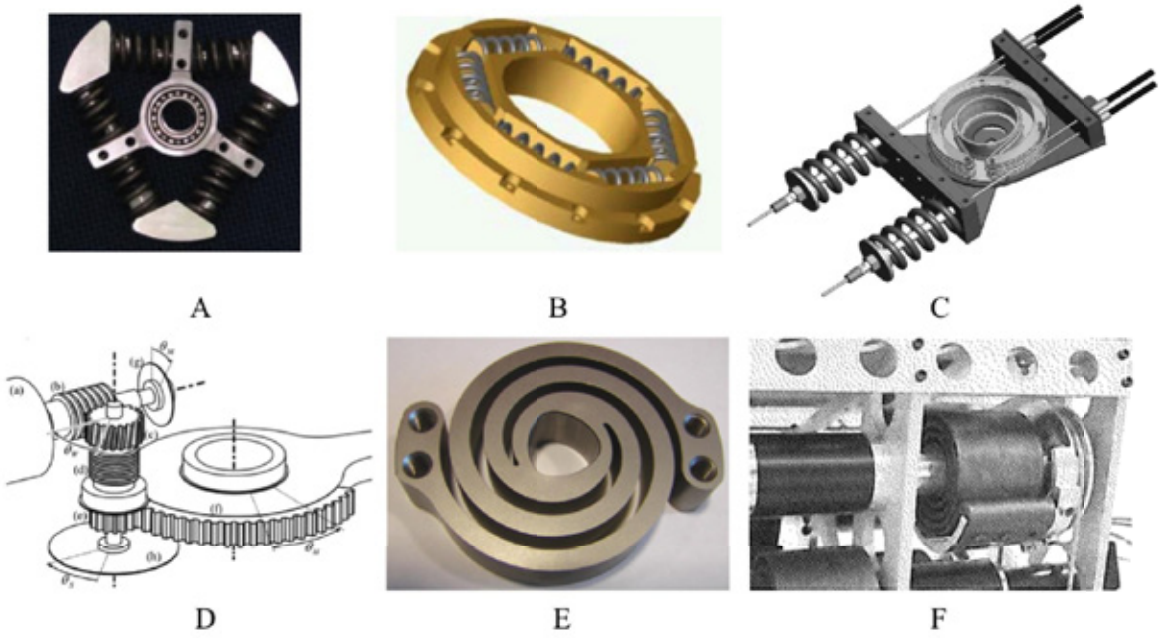

Fig. 2. Examples of compliant components for rotary SEA prototypes: [11] (A), [12] (B), [17] (C), [10] (D), [14] (E), [16] (F).

safety. An optimal stiffness can be determined as a trade-off between two requirements: *i)* increasing the Large Force Bandwidth (LFB) [4] and *ii)* reducing the intrinsic mechanical impedance. Additionally, since the applied torque is inferred from the spring deflection, spring stiffness has also an impact on the torque measurement resolution. For a given resolution of the measurement elements, a more compliant component allows a smaller quantization of the torque signal, thus improving the accuracy of torque estimation. Moreover, a high linearity in the torque vs. angle relationship is desirable in order to guarantee an accurate torque estimation and consequent control performance. For this same reason, also residual deflection (at zero delivered torque) and hysteresis should be avoided.

It is particularly difficult to define the optimal value of the physical elasticity of a SEA to be used in a wearable robot for gait assistance. The analysis of the literature on wearable robotics [9, 10, 14, 15] and the biomechanics studies addressing the measurement of the viscoelastic properties of lower limbs joints [19, 20] show heterogeneous results for each addressed joint of the lower limbs. Given this lack of evidence, the subsystem providing the desired series elasticity should possibly be modular, so to render a variety of desired stiffness values by properly interconnecting (e.g. in series or parallel) the basic elastic building blocks.

This paper presents a novel compact torsional spring for SEAs, designed as a single monolithic component; this element is suitable to be used as the basic unit for creating multiple series/parallel interconnections. The basic requirements for the design of the torsional spring are described in Section 2, while in Section 3 the applied methodology and the design phase are reported. The experimental characterization is presented in Section 4. Section 5 is dedicated to discussion and conclusions.

2 Design Requirements

The elastic module presented in this paper is the building block for creating, via a proper arrangement, the spring to be included in a SEA actuating an orthosis for knee flexion/extension assistance, as needed by elderly subjects with age-related motor performance decay. A number of gait features are influenced by aging. The gait of senior people is mainly characterized by decreased gait velocity, caused by a decreased step length [21] and by an increased stance time [22]. Elderly people generally have a more conservative gait pattern, i.e. a lower preferred walking speed [23] and shorter steps [24]. Considering the slow-walking data set described in [25], the maximum instantaneous power exerted by the knee joint is about 40 W, with a maximum torque of 29 N·m and a RMS value of 20 N·m. As design target, the new SEA should provide an assistive torque not larger than the 50% of the peak torque developed during overground walking (15 N·m).

As already mentioned, SEA torque regulation can be conveniently achieved by position- or velocity-controlling the motor [7, 18, 26]. In order to avoid non-linear control schemes and to allow homogeneous regulation capability over the whole range of deliverable torques, a linear torque vs. angle characteristic is desirable. Indeed, non-linear relationships would imply an increased sensitivity to motor positioning inaccuracies, thus possibly implying regulation errors in case of large torques. Moreover, the elastic component should be connected to the load in a direct drive configuration, so to avoid transmissions non-linearities compromising force fidelity. The target stiffness value has to be selected as a trade-off between low intrinsic compliance and

accurate torque control in a given frequency bandwidth. The desirable physical stiffness values of SEAs for locomotion assistance, as retrieved from literature, may range from 100 to 300 N·m/rad [9, 10, 14, 15]. The suitability of these values has been demonstrated also by theoretical analyses [4] and recent simulation studies [27], on the basis of realistic velocity and current limitations for DC motors. From previous considerations, a stiffness of 200 N·m/rad and a peak admissible torque of 15 N·m are taken as target values for our design.

In order to minimize weight and size, a compact disc-shaped design is pursued. A small encumbrance of the module is mandatory when basic elements must be interconnected (e.g. mounted in parallel or in series) to achieve configurations exhibiting the desired peak torque/stiffness. The selected design implies the transfer of torque between an outer ring (diameter 100 mm) and an inner ring (diameter 12 mm). Compliance is obtained by connecting the two rings with flexible elements, whose shape is defined through the methodology described in Section 3. The minimum thickness of the flexible elements is set to 0.1 mm due to the constraints imposed by the fabrication technology (Wire Electrical Discharge Machining, WEDM).

Both the main design requirements (i.e. 15 N·m peak torque; 200 N·m/rad stiffness) are hardly satisfied by a single elastic element. Under this regard, a parallel mounting of two elastic modules is beneficial because, in this configuration, each module has to withstand only a peak torque of 7.5 N·m while exhibiting a torsional stiffness reduced to 100 N·m/rad. In other words, both the maximum torque and the expected stiffness are reduced to half their original value, thus easing the design of the elastic module. The other relevant design requirements for the single elastic module are reported in Tab. 1. In the following, the design of the single basic element of the parallel configuration will be described.

3 Methodology

The design of the elastic modules relies on an iterative Finite Element Method (FEM) simulations-based process, described by the flowchart in Fig. 3.

The first step consists in choosing a set of topologies for the elastic module. Each topology is in one-to-one correspondence with the set of parameters necessary to define a certain morphological implementation. Given n, the number of variable parameters, and $(x_i^{MIN} \; x_i^{MAX})$, the range of admissible values for the i^{th} parameter, a n-dimensional search space is thus defined. Within this domain, an initial-guess value is assigned to each parameter. The corresponding model (morphology) is then imported in a Finite Element Analysis (FEA) software to check if the design criteria are satisfied (compliance, robustness). If not, two possibilities arise:

1. to change the parameters values within the range defined for the considered topology (i.e. by adding and removing material so to obtain the desired stiffness with a homogeneous stress distribution);
2. to change topology and reiterate the process, if the search space for the selected topology is considered to be adequately searched (maximum number of iterations reached for each topology, in our case set to twenty).

In the positive case (i.e. design criteria satisfied) the optimization phase ends, and the chosen morphology is considered as an acceptable design.

It is worth noting that the described methodology does not guarantee that the whole n-dimensional search space is exhaustively spanned, but it is instead oriented to achieve at least one practical design that satisfies the objectives described in previous sections. Moreover, the outcome of the FEA-assisted iterative process is affected by the contribution of the designer, both in the initial phase, where the design problem is defined, and in the step-by-step refinement process.

Fig. 3. Flowchart describing the spring design methodology.

Table 1. Design requirements for the elastic module.

Parameter	Value
Stiffness	100 N·m/rad
Max torque	7.5 N·m
Max deflection	0.075 rad
Max outer diameter	100 mm
Max thickness	5 mm
Max weight	100 g

In order to evaluate intermediate design solutions that do not meet the requirements stated above, and to drive the process towards the topologies that are more adequate to provide a suitable solution, the criterion of maximization of the specific energy storable in safe stress conditions is employed. The specific energy (e_{el}) stored in the elastic module is defined as:

$$e_{el} = \frac{1}{2}\frac{k\Delta\theta^2}{M} \quad (1)$$

where k is the torsional stiffness, $\Delta\theta$ the rotation angle and M the module mass. The torsional stiffness is calculated as the ratio between the applied torque and the corresponding deformation angle, calculated from FEM simulations. A topology is discarded if the design criteria, described in Section 2, could not be satisfied after twenty iterations.

Figure 4 shows the three elastic modules topologies taken into account. The solid circles represents the inner and the outer rings, whose diameters are fixed. The dotted ellipses represent the flexible elements. The number and arrangement of the flexible elements define a specific topology, while their dimensional parameters (i.e. length, width, distance from the center) define a specific morphological implementation.

3.1 Design

The first step in the design process is to define the set of topologies. Following the principle of incrementally increasing complexity, it was decided to start from a set of three topologies with increasing geometric (i.e. number of optimization parameters) and manufacturing cost (i.e. length of the WEDM path). Moreover, a symmetric structure was chosen in order to assure that a torque produces a rotation, without translation of the inner ring with respect to the outer ring. The basic topologies are described in Fig. 4. One may argue that the simplest topology, leading to a spiral or double spiral morphology, was not taken into account. This is true, and the decision came from the observation that this geometry, already investigated in [14], is not a promising candidate to meet our requirements in terms of desired stiffness and robustness and to assure the target level of flexibility for the design of the elastic module.

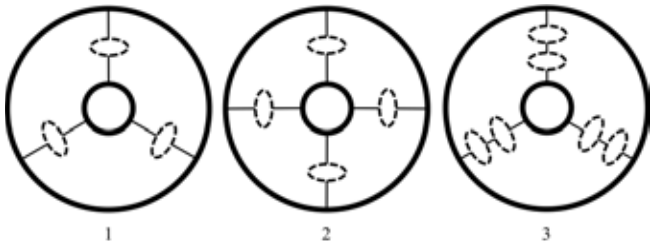

Fig. 4. Elastic modules topologies taken into account. The solid circles represent the rigid inner and outer rings, while dotted ellipses represent the flexible elements.

After that, the shape of the flexible elements represented in Fig. 4 was defined. Flexible elements are arched lamellae disposed in a closed loop, acting as curved thin beams.

Considering each replication of lamellae blocks (as shown in Fig. 5 using an arbitrary morphology based on topology 3), the distance of the m lamellae from the center are labeled with R_j ($j = 1 \quad m$) and the width of the lamellae with s_j ($j = 1 \quad m$). The width of the interconnections between lamellae and between lamellae and inner/outer rings are indicated with w_j ($j = 1 \quad m\ 2+1$), the width of the arches joining two different lamellae with p_j ($j = 1 \quad m\ 2$) and the aperture angle of the lamellae blocks with α. D_j ($j = 1\ 2$) define the diameter of the inner and outer rings. Table 2 reports an example (related to topology 3) of the description of the design parameters, with the definition of the lower and upper bounds and the minimum increment adopted to explore the search space. Constant parameters comprise the diameter of the inner hole, the outer diameter (external ring) and the thickness of the torsional spring (not shown in Fig. 5).

3.1.1 FEM Simulations

FEM static stress-strain analyses have been performed to evaluate alternative designs. Static large displacement FEM analysis (COMSOL Multiphysics 3.5, Comsol AB) were performed with clamped inner ring (red dotted circles in Fig. 6) and outer ring loaded by a tangential distributed force (f, black arrows in Fig. 6) equivalent to a pure torque (M):

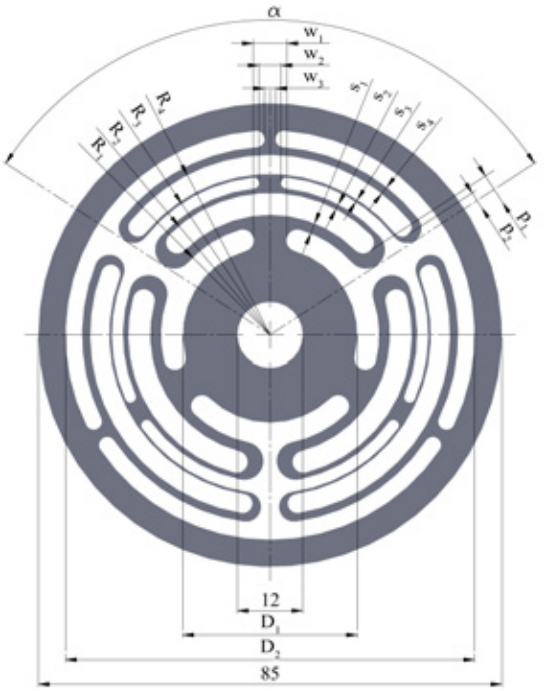

Fig. 5. An arbitrary morphology based on topology 3. Spring thickness is 3 mm.

Table 2. Search space for the optimization problem of topology 3. For each parameter, the search space is defined, based on the upper and lower bound and minimum increment adopted in the optimization process. R_j, s_j, w_j, p_j and D_j are in [mm], α is in [rad].

Parameter	Min.	Max.	Min. increment
R_1	20	24	0.5
R_2	23	27	0.5
R_3	26	30	0.5
R_4	29	33	0.5
s_1	0.1	2	0.1
s_2	0.1	2	0.1
s_3	0.1	2	0.1
s_4	0.1	2	0.1
w_1	3	10	0.5
w_2	2	8	0.5
w_3	2	8	0.5
p_1	0.1	2	0.1
p_2	0.1	2	0.1
D_1	30	35	1
D_2	70	75	1
α	0.87	0.99	0.02

$$f = \frac{M}{2\pi \cdot \Delta z \cdot R^2} \tag{2}$$

where R is the outer radius and Δz the thickness.

A one layer swept tetrahedral mesh has been used (Fig. 6). The 3D subdomain has been meshed starting from a source face and then sweeping the resulting face mesh along the subdomain to the opposite target face. The distribution method is linear with an element ratio equal to 1. The mesh is refined around higher curvature elements (e.g. lamellae and holes), while it is coarser in correspondence of the external ring, where lower stresses are expected. A stationary non linear solver (SPOOLES) with a relative tolerance of 10^{-6} has been used.

3.1.2 Design results

Figure 7 reports the maximum e_{el} for the best morphology obtained after the iterative refinement process for each of the three analyzed topologies. Table 3 provides an

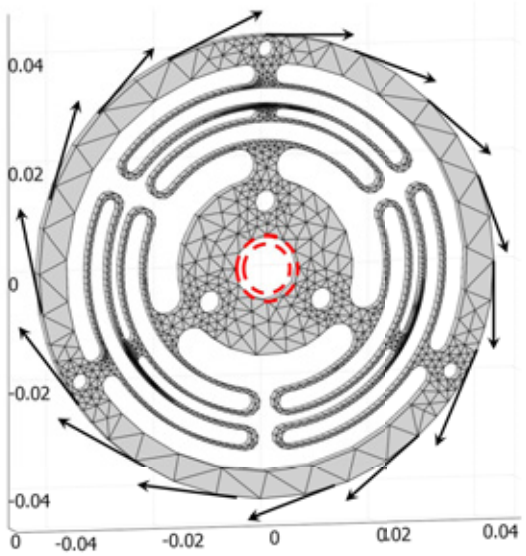

Fig. 6. Boundary conditions and swept mesh. The internal ring is fixed (double dashed line) while tangential forces (solid arrows) are applied to the outer ring. Dimensions are in [m].

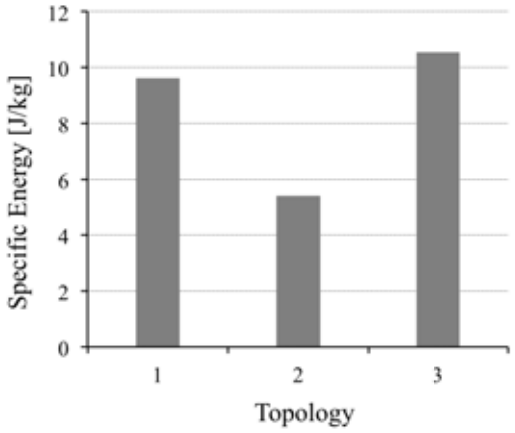

Fig. 7. Specific energy for the three investigated topologies. For each topology the best morphological implementation, obtained through the design refinement process, is considered. No morphology deriving from topology 2 reached the design objectives after the specified maximum number of design iterations (20).

overview of the best morphologies obtained after the optimization phase implementing the three considered topologies.

Considering this comparison criterion and that no valid design could be obtained for topology 2 after twenty design iterations, it is assumed that the fittest solution can be obtained through a parameter optimization based on topology 3. Such configuration includes three replications of two couples of lamellae, arranged at 2 3π as shown in Fig. 5. In Fig. 8, 1:1 elastic module deformation and von Mises stress as obtained by the FEM simulation are reported under an applied torque of 7.68 N·m. The maximum resultant von

Table 3. Parameters defining the best morphologies produced by the optimization, for each of the three considered topologies. R_j, s_j, w_j, p_j and D_j are in [mm], α is in [rad]. N is the number of angular replication of compliant blocks, m is the number of lamellae (2 for each block).

Parameter	Topology 1	Topology 2	Topology 3
R_1	18	18	23
R_2	26.5	26.5	27
R_3	N/A	N/A	29.5
R_4	N/A	N/A	33
s_1	1.1	1	0.6
s_2	0.9	0.8	0.5
s_3	N/A	N/A	0.6
s_4	N/A	N/A	0.5
w_1	5	5	5
w_2	N/A	N/A	3
w_3	4	4	4
p_1	1.1	1	0.6
p_2	N/A	N/A	0.6
D_1	32	32	32
D_2	75	75	75
α	2.0	1.5	2.0
N	3	4	3
m	2	2	4

Mises stress is 1.27 GPa. Considering that the yield stress of the selected material (σ_y) is 1.91 GPa a safety factor of 1.5 is achieved. The external ring rotation is 0.083 rad, corresponding to a torsional stiffness of 92 N·m/rad.

Overall, 12 simulations have been performed applying a torque from 0.64 N·m to 7.68 N·m with a step of 0.64 N·m to analyze the linearity of the torque vs. rotation relationship. The resulting values for each simulation are reported with a solid line in Fig. 13. The simulated elastic module exhibits the expected linear characteristics, with a R-square value of 0.999. The specific energy stored in the component is 11.69 J/kg.

The optimized module, shown in Fig. 9, has been manufactured by WEDM from Vascomax C-300 (maraging steel 300, Young modulus of 186 GPa, yield stress of 1.91 GPa and ultimate tensile strength of 1.96 GPa after an aging treatment of 4 hours at 482°C). In the fourth column of Tab. 3 the optimized module dimensions are reported. Holes on the outer and inner rings are used for the connections with the gearmotor and the output shaft respectively, thus embodying the Series Elastic Actuation architecture.

Fig. 9. Frontal view of the custom made torsional elastic module. Diameter: 85 mm. Thickness: 3 mm. Weight: 61.5 g.

4 Characterization of the Torsional Elastic Module

The experimental characterization of the torsional elastic module has been conducted using a custom-made dynamometric test bed. Figure 10 reports a scheme describing the test bed operating principle, which involves the use of a gear reduction stage.

The load is applied trough a steel wire (Fig. 10–1, diameter 0.6 mm) connected to the moving crosshead of the Instron testing machine (Instron 3365, INSTRON Inc, Norwood, MA, US load cell, Full Scale: 500 N, accuracy in force regulation of 0.5%) and to a pulley (Fig. 10–2, radius 80 mm) connected to the secondary shaft (Fig. 10–3). The resulting torque is transmitted to the primary shaft (Fig. 10–4) through a 4:1 gear transmission (Fig. 10–5). The primary

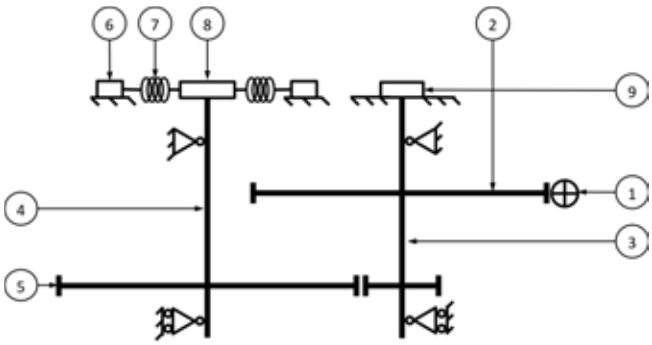

Fig. 10. Schematic representation of the operating principle of the custom-made dynamometric test bed. 1: wire connected to Instron testing machine, 2: pulley, 3: primary shaft, 4: secondary shaft, 5: gear transmission, 6: external ring, 7: torsional elastic elements, 8: internal ring, 9: encoder.

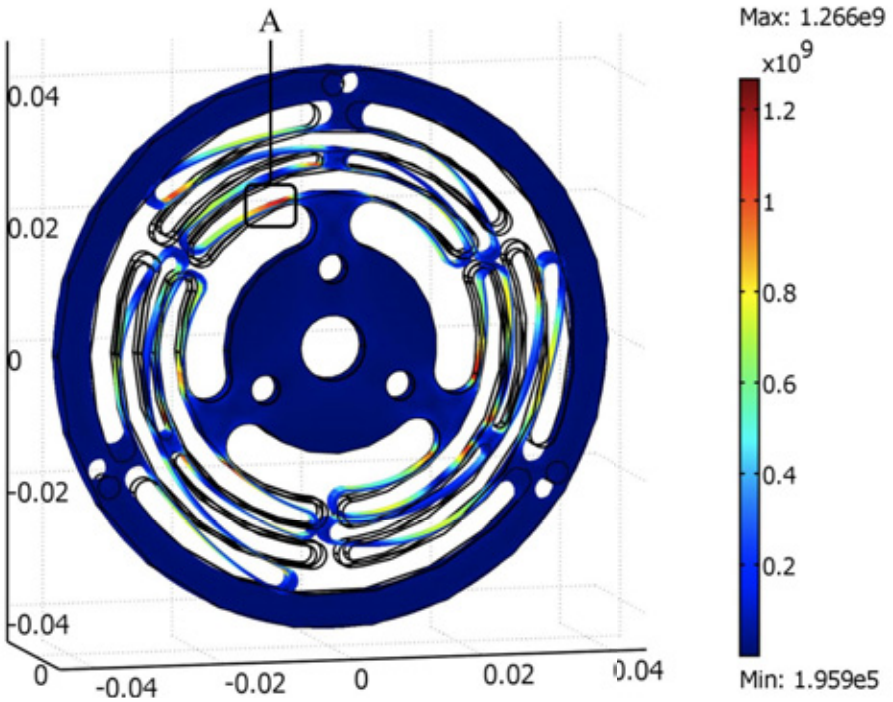

Fig. 8. von Mises stress in [Pa] and 1:1 module deformation. Dimensions in [m].

shaft and the inner ring of the elastic module (Fig. 10–8) are connected by a shaped shaft-hub coupling, while the outer ring (Fig. 10–6) is fixed to the frame. The angular deflection is measured by an incremental magnetic encoder placed on the secondary shaft (not reduced). The 4:1 reduction ratio allows a resolution in the measurement of the deflection (and consequently in the evaluation of stiffness) four times higher compared to the nominal resolution of the employed encoder. The magnetic incremental encoder (Fig. 10–9) comprises two elements: a reading sensor (ASM PMIS4 480 kHz) fixed to the frame and a magnetic wheel (ASM PMIR7-20-64-M-20) connected to the secondary shaft, enabling a resolution in deflection measurement of $7.7 \cdot 10^{-4}$ rad.

In Fig. 11 a rendering of the test bed is shown. Figure 12 shows the elastic module mounted on the test bed in the unloaded condition and in deformed state.

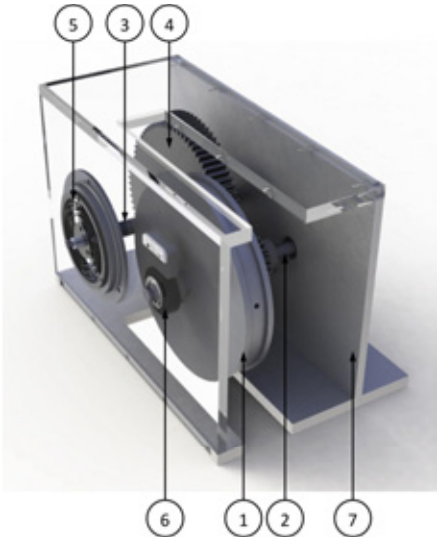

Fig. 11. 3D rendering of the dynamometric test bed (frame surfaces in transparency and wire connected to Instron not shown). 1: pulley, 2: primary shaft, 3: secondary shaft, 4: gear transmission, 5: torsional elastic module, 6: encoder, 7: frame.

4.1 Experimental results

The torsional elastic module has been experimentally characterized by applying increasing values of torque from 0.64 N·m to 7.68 N·m, with increments of 0.64 N·m. These values correspond to forces applied by the Instron from 2 N to 24 N, with increments of 2 N. In Fig. 13, the torque vs. rotation characteristics of the real and simulated modules are plotted. Five tests have been performed for each value of applied torque, allowing the element to recover the unperturbed position after each measure; the resulting average values and 95% confidence intervals are reported in Fig. 13. Linear regression for data acquired during the characterization phase is represented with a dotted line (R^2 = 0.998). On the same plot, data from FEM simulations are interpolated with a linear regression represented with a solid line (R^2 = 0.999). FEM simulations data would predict a stiffness k_{sim}= 92 N·m/rad, while the measurements indicated a stiffness k_{real} = 98 N·m/rad, corresponding to an error between simulated data and measured data, calculated as $(k_{real} - k_{sim})\ \ k_{sim} \cdot 100$, equal to 6.5%.

Although not customarily performed for the intended application, a preliminary fatigue analysis has been performed according to [28]. The analysis has been conducted

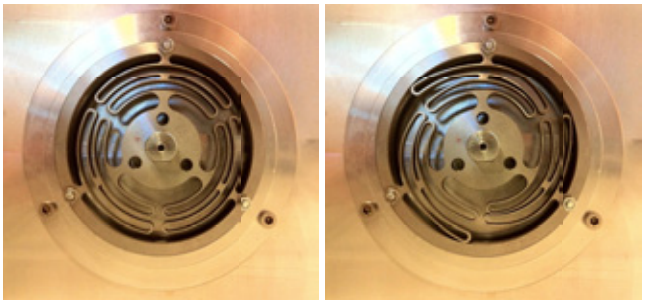

Fig. 12. Elastic module in unloaded state (left) and in deformed state (right), applied torque: 7.68 N·m.

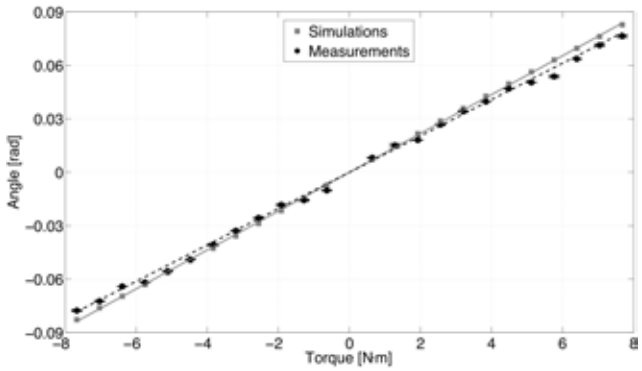

Fig. 13. Simulated data are represented with square dots, while experimental data are represented with circle dots. The stiffness (calculated as the inverse of the slope of the linear regression curves) is equal to 92 N·m/rad for the simulated elastic module and 98 N·m/rad for the real device.

considering the most stressed region in the elastic component (region A in Fig. 8). A sinusoidal load with a peak value of 7.68 N·m and a root mean square value of 5.2 N·m has been considered. The fatigue limit (σ_f) for infinite endurance (i.e. $> 10^6$ cycles) can be evaluated as:

$$\sigma_f = 0\,5 \cdot \sigma_R \cdot C_L \cdot C_G \cdot C_S \tag{3}$$

where σ_R is the ultimate tensile strength of the material, C_L is the load coefficient ($C_L = 1$ for tension/compression and bending), C_G is the stress gradient coefficient ($C_G = 0\,9$ for thicknesses below $10\,mm$) and C_S is the surface finishing coefficient ($C_S = 0\,9$ for ground surfaces with $R_a = 0\,8$). The evaluated fatigue limit is 0.79 GPa, which is close but smaller than the maximum expected von Mises stress (0.84 GPa). Since the fatigue limit is quite close to the maximum von Mises stress, the evaluation of the actual fatigue life deserves further experimental investigation, as discussed in Section 5.

5 Discussion and conclusions

In this paper the design of a monolithic torsional elastic module for rotary SEAs was presented. The torsional module is able to withstand a maximum torque of 7.68 N·m, with a constant torsional stiffness of 98 N·m/rad, in good agreement with FEM simulations, which predicted a stiffness value of 92 N·m/rad. In Table 4, the main mechanical properties of the torsional module are reported, as experimentally characterized.

Table 4. Properties of the basic compliant element.

Parameter	Value
Stiffness	98 N·m/rad
Max torque	7.68 N·m
Max deflection	0.078 rad
Outer diameter	85 mm
Thickness	3 mm
Weight	61.5 g
Specific stored energy	11.69 J/kg

The designed elastic element is conceived as the basic building block, which can be arranged in several ways by serial and parallel interconnections. In the specific application described in Section 2, two identical torsional elastic modules are simply connected in parallel, providing an equivalent stiffness of 196 N·m/rad and withstanding a maximum torque of 15.36 N·m. Under this regard, the parallel configuration is helpful, because it allows splitting the total torque between the two elastic modules mounted in parallel, each module withstanding half of the total torque. Figure 14–A depicts a cross section of the mentioned parallel configuration. Also series interconnections can be simply arranged as in Fig. 14–B. In this case two elastic packs, each including elastic modules in parallel configuration, are connected in series, thus providing an equivalent stiffness of 98 N·m/rad and a maximum torque of 15.36 N·m. In this configuration, each pack is loaded by a maximum torque of 15.36 N·m and undergoes an equal maximum deflection of 0.156 rad.

Being a fundamental component of the SEA, the deflection of the torsional spring must be carefully measured during actuator operation. This can be achieved by mounting two encoders on the input and output shafts of the elastic modules pack, and estimating its deformation by subtracting the two independent measurements. This allows to implement the basic torque control scheme described in Fig. 1. Under this regard, it is important to define the basic requirements for the angular sensors, whose measurements can be used to infer the instantaneous torque applied to the load. Given K, the equivalent output stiffness of the spring put in series between the actuator and the load ($K = f(k)$, f the function defined by the connection topology of basic elements with stiffness k), and p the number of bits of the encoders used to measure the angle of the input and output shafts of the spring, the theoretical torque measurement quantization $\Delta\tau_{meas}$ is given by:

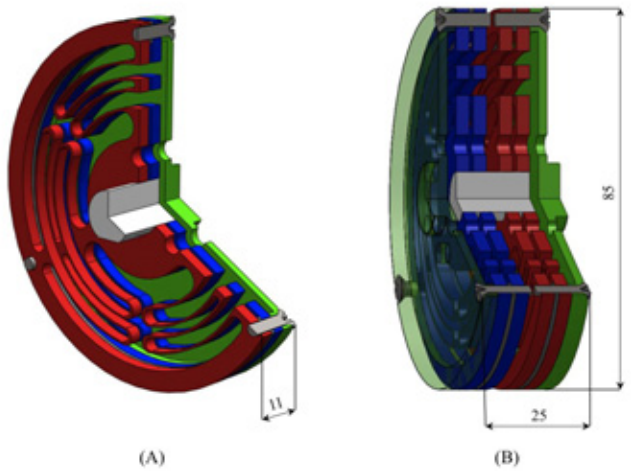

Fig. 14. (A) Section view of a parallel configuration of two basic elastic modules. The elastic modules are shown in red and in blue, the output shaft connecting the internal rings of the springs with the load is shown in white, and the flange connecting the external rings of the modules and the gearmotor is in green. Using the basic element (specs reported in Tab. 4), the equivalent output stiffness is 196 N·m/rad and the max supported torque 15.36 N·m. (B) Section view of a design including the series connection of two parallel modules packs (shown in blue and in red). The white shaft connects the internal rings of the two modules packs, while the green flanges, acting as input and output ports of the elastic system, connect the external rings of the two modules packs. The equivalent stiffness between input and output is 98 N·m/rad and the maximum supported torque 15.36 N·m.

$$\Delta\tau_{meas} = \frac{K \cdot 2\pi}{2^p} \tag{4}$$

Inverting Eq. 4, and considering a minimum resolution of torque measurement of 0.1 N·m for wearable robotics applications [15], the minimum resolution required to the encoders ranges from 13 to 15 bit, when K is between 100 and 300 N·m/rad. Taking into account these considerations, the measurement of the spring deflection can be achieved in the actual design by employing commercially available sensors.

The fatigue analysis does not assure an infinite fatigue life of the elastic component, because the evaluated fatigue limit (0.79 GPa) is only slightly below the calculated maximum von Mises stress (0.84 GPa). Although the adopted calculation scheme is slightly conservative [28], an experimental characterization of the fatigue resistance of the elastic module will be performed in future works.

The custom elastic element developed and characterized in this paper can be applied wherever actuators compliance is crucial, as in robots where a safe pHRI is mandatory. Humanoid and walking robots can also benefit from elastic joints for energetic efficiency and biomimetic behaviors. Future works will be focused on the dynamic characterization of the elastic component, which will be included in a SEA prototype under development.

Acknowledgements

This work was supported by the FP7 FET Proactive Initiative Embodied Intelligence of the European Commission, project no. ICT-2007.8.5-231451 - EVRYON (EVolving morphologies for human-Robot sYmbiotic interactiON).

The authors wish to thank Mr. Augusto Cozzi for his help in the preliminary work related to the experimental characterization of the spring.

References

[1] De Santis, A., Siciliano, B., De Luca, A., and Bicchi, A., 2008. "An atlas of physical human-robot interaction". *Mechanism and Machine Theory,* **43**(3), pp. 253–270.

[2] Van Ham, R., Sugar, T., Vanderborght, B., Hollander, K., and Lefeber, D., 2009. "Compliant actuator designs". *Robotics & Automation Magazine, IEEE,* **16**(3), pp. 81 – 94.

[3] Pratt, G., and Williamson, M., 1995. "Series elastic actuators". In Proc. IEEE/RSJ International Conference on Intelligent Robots and Systems "Human Robot Interaction and Cooperative Robots", Vol. 1, pp. 399 – 406 vol.1.

[4] Robinson, D., 2000. "Design and analysis of series elasticity in closed-loop actuator force control". PhD Thesis, Massachusetts Institute of Technology, Cambridge, MA, June.

[5] Paluska, D., and Herr, H., 2006. "The effect of series elasticity on actuator power and work output: Implications for robotic and prosthetic joint design". *Robotics and Autonomous Systems,* **54**(8), pp. 667–673.

[6] Hurst, J., Rizzi, A., and Hobbelen, D., 2004. "Series elastic actuation: Potential and pitfalls". *International Conference on Climbing and Walking Robots*.

[7] Vallery, H., Veneman, J., van Asseldonk, E., Ekkelenkamp, R., Buss, M., and van der Kooij, H., 2008. "Compliant actuation of rehabilitation robots: benefits and limitations of series elastic actuators". *IEEE Robotics & Automation Magazine,* **15**(3), pp. 60–69.

[8] Pratt, G., 2000. "Legged robots at MIT: what's new since raibert?". *IEEE Robotics & Automation Magazine,* **7**(3), pp. 15 – 19.

[9] Veneman, J. F., Ekkelenkamp, R., Kruidhof, R., van der Helm, F., and van der Kooij, H., 2006. "A series elastic- and bowden-cable-based actuation system for use as torque actuator in exoskeleton-type robots". *The International Journal of Robotics Research,* **25**(3), pp. 261–281.

[10] Kong, K., Bae, J., and Tomizuka, M., 2010. "A compact rotary series elastic actuator for knee joint assistive system". In Proc. 2010 IEEE International Conference on Robotics and Automation, pp. 2940 – 2945.

[11] Tsagarakis, N., Laffranchi, M., Vanderborght, B., and

Caldwell, D., 2009. "A compact soft actuator unit for small scale human friendly robots". In Proc. IEEE International Conference on Robotics and Automation, pp. 4356 – 4362.

[12] Yoon, S., Kang, S., Kim, S., Kim, Y., Kim, M., and Lee, C., 2003. "Safe arm with mr-based passive compliant joints and visco-elastic covering for service robot applications". In Proc. IEEE/RSJ International Conference on Intelligent Robots and Systems, Vol. 3, pp. 2191 – 2196.

[13] Wyeth, G., 2008. "Demonstrating the safety and performance of a velocity sourced series elastic actuator". In Proc. IEEE International Conference on Robotics and Automation, pp. 3642 – 3647.

[14] Lagoda, C., Schouten, A., Stienen, A., Hekman, E., and van der Kooij, H., 2010. "Design of an electric series elastic actuated joint for robotic gait rehabilitation training". In Proc. 3rd IEEE RAS and EMBS International Conference on Biomedical Robotics and Biomechatronics, pp. 21 – 26.

[15] Stienen, A., Hekman, E., ter Braak, H., Aalsma, A., van der Helm, F., and van der Kooij, H., 2010. "Design of a rotational hydroelastic actuator for a powered exoskeleton for upper limb rehabilitation". *IEEE Transactions on Biomedical Engineering,* **57**(3), pp. 728 – 735.

[16] Knox, B., and Schmiedeler, J. P., 2009. "A unidirectional series-elastic actuator design using a spiral torsion spring". *ASME Journal of Mechanical Design,* **131**(125001), pp. 1–5.

[17] Veneman, J., Ekkelenkamp, R., Kruidhof, R., van der Helm, F., and van der Kooij, H., 2005. "Design of a series elastic- and bowden cable-based actuation system for use as torque-actuator in exoskeleton-type training". In Proc. 9th IEEE International Conference on Rehabilitation Robotics, pp. 496 – 499.

[18] Wyeth, G., 2006. "Control issues for velocity sourced series elastic actuators". In Proc. Australasian Conference on Robotics and Automation.

[19] Zhang, L., Nuber, G., Butler, J., Bowen, M., and Rymer, W., 1998. "In vivo human knee joint dynamic properties as functions of muscle contraction and joint position". *Journal of biomechanics,* **31**(1), pp. 71–76.

[20] Loram, I., and Lakie, M., 2002. "Direct measurement of human ankle stiffness during quiet standing: the intrinsic mechanical stiffness is insufficient for stability". *The Journal of Physiology,* **545**(3), pp. 1041–1053.

[21] JudgeRoy, J. O., Davis, B., and Ounpuu, S., 1996. "Step length reductions in advanced age: The role of ankle and hip kinetics". *The Journals of Gerontology Series A: Biological Sciences and Medical Sciences,* **51**(6), pp. 303–312.

[22] Murray, M. P., Kory, R. C., and Clarkson, B. H., 1969. "Walking patterns in healthy old men". *Journal of Gerontology,* **24**(2), pp. 169–178.

[23] Rose, J., and Gamble, J., 2005. *Human Walking*. Eds. Lippincott USA.

[24] Menz, H. B., Lord, S. R., and Fitzpatrick, R. C., 2003. "Age-related differences in walking stability". *Age and Ageing,* **32**(2), pp. 137–142.

[25] Winter, D., 2009. *Biomechanics and Motor Control of Human Movement*. Wiley.

[26] Sensinger, J. W., and ff. Weir, R. F., 2006. "Improvements to series elastic actuators". In Proc. 2nd IEEE/ASME International Conference on Mechatronic and Embedded Systems and Applications, pp. 1–7.

[27] Tagliamonte, N., Sergi, F., Carpino, G., Accoto, D., and Guglielmelli, E., 2010. "Design of a variable impedance differential actuator for wearable robotics applications". In Proc. IEEE/RSJ International Conference on Intelligent Robots and Systems, pp. 2639 – 2644.

[28] Juvinall, R. C., and Marshek, K. M., 2006. *Fundamentals of machine component design*. John Wiley & Sons, Chap. 8, pp. 290–347.